

LRP1 is a master regulator of tau uptake and spread

<https://doi.org/10.1038/s41586-020-2156-5>

Received: 8 October 2019

Accepted: 27 February 2020

Published online: 01 April 2020

 Check for updates

Jennifer N. Rauch¹, Gabriel Luna¹, Elmer Guzman¹, Morgane Audouard¹, Collin Challis², Youssef E. Sibih¹, Carolina Leshuk¹, Israel Hernandez¹, Susanne Wegmann³, Bradley T. Hyman⁴, Viviana Gradinaru², Martin Kampmann^{5,6} & Kenneth S. Kosik^{1✉}

The spread of protein aggregates during disease progression is a common theme underlying many neurodegenerative diseases. The microtubule-associated protein tau has a central role in the pathogenesis of several forms of dementia known as tauopathies—including Alzheimer's disease, frontotemporal dementia and chronic traumatic encephalopathy¹. Progression of these diseases is characterized by the sequential spread and deposition of protein aggregates in a predictable pattern that correlates with clinical severity². This observation and complementary experimental studies^{3,4} have suggested that tau can spread in a prion-like manner, by passing to naive cells in which it templates misfolding and aggregation. However, although the propagation of tau has been extensively studied, the underlying cellular mechanisms remain poorly understood. Here we show that the low-density lipoprotein receptor-related protein 1 (LRP1) controls the endocytosis of tau and its subsequent spread. Knockdown of *LRP1* significantly reduced tau uptake in H4 neuroglioma cells and in induced pluripotent stem cell-derived neurons. The interaction between tau and LRP1 is mediated by lysine residues in the microtubule-binding repeat region of tau. Furthermore, downregulation of *LRP1* in an in vivo mouse model of tau spread was found to effectively reduce the propagation of tau between neurons. Our results identify LRP1 as a key regulator of tau spread in the brain, and therefore a potential target for the treatment of diseases that involve tau spread and aggregation.

Recent work has highlighted the importance of heparan sulfate proteoglycans (HSPGs) in tau uptake^{5,6}, and low-density lipoprotein receptors (LDLRs) are known to work in conjunction with HSPGs⁷. On the basis of this knowledge, we set out to test whether any members of the LDLR family could influence tau internalization. Using CRISPR interference (CRISPRi) technology, the expression of genes encoding various members of the LDLR family (*LRP1*, *LRP1B*, *LRP2*, *LRP5*, *LRP6*, *LDLR* and *VLDLR*; Extended Data Fig. 1c) was efficiently repressed in H4 neuroglioma cells, and the ability of these cells to endocytose monomeric tau was assessed⁵ (Fig. 1a, b). Genetic silencing of *LRP1* almost completely blocked the uptake of full-length soluble monomeric tau (2N4R isoform), whereas no significant effect was found upon silencing any other LDLR family member (Fig. 1b). Different mechanisms have been proposed for the uptake of soluble and of aggregated tau⁸. However, *LRP1* knockdown was also sufficient to inhibit the uptake of tau oligomers, and reduced but did not completely inhibit the uptake of sonicated tau fibrils (Fig. 1c). The uptake of a disease-relevant mutant of tau and of phosphorylated tau was also affected by *LRP1* knockdown (Extended Data Fig. 1d). To show that *LRP1* knockdown was specific for tau endocytosis, we analysed the uptake of transferrin in H4 cells; *LRP1* knockdown was found to have no effect on transferrin endocytosis (Fig. 1d). Knockdown of *LRP1* also prevented uptake of the smaller

isoforms of tau (ON3R, ON4R, 1N3R, 1N4R and 2N3R) as well as fragments of tau that contain only the microtubule-binding repeat region (K18, 4 repeats; K19, 3 repeats; Fig. 1e). These findings highlight the microtubule-binding region as the potential interaction site.

To further support the results from the *LRP1*-knockdown cell lines, a well-known LRP1-binding protein—receptor-associated protein (RAP)—was used as a competitor for tau uptake in wild-type H4 cells. RAP is a small, 39 kDa chaperone for LRP1 that is known to bind tightly to LRP1 (dissociation constant, $K_D = 9$ nM)⁹. Increasing concentrations of RAP in the culture medium, added concurrently with tau, were highly effective at inhibiting the uptake of both full-length tau and K18 tau (half-maximum inhibitory concentration, $IC_{50} = 4.9$ nM and 9.6 nM, respectively); however, they did not influence the internalization of transferrin (Fig. 2a). We next introduced point mutations at residues of RAP that are required for its interaction with LRP1¹⁰; the mutation of lysines 256 and 270 to alanine (to form the mutant RAP(K256A/K270A), hereafter denoted mtRAP) was sufficient to reduce this competitive effect (Extended Data Fig. 2a, b).

In an attempt to understand how tau may interact with LRP1, we examined known crystal structures of members of the LDLR family bound to their ligands^{11,12}. LRP1 (and other members of the LDLR family) contain cysteine-rich complement-type repeats that bind and internalize their

¹Neuroscience Research Institute, Department of Molecular, Cellular, and Developmental Biology, University of California, Santa Barbara, CA, USA. ²Division of Biology and Biological Engineering, California Institute of Technology, Pasadena, CA, USA. ³German Center for Neurodegenerative Diseases (DZNE), Berlin, Germany. ⁴Massachusetts General Hospital, Harvard Medical School, Boston, MA, USA. ⁵Institute for Neurodegenerative Diseases, Department of Biochemistry and Biophysics, The California Institute for Quantitative Biomedical Research, Quantitative Biosciences Institute, University of California, San Francisco, CA, USA. ⁶Chan Zuckerberg Biohub, San Francisco, CA, USA. ✉e-mail: kenneth.kosik@lifesci.ucsb.edu

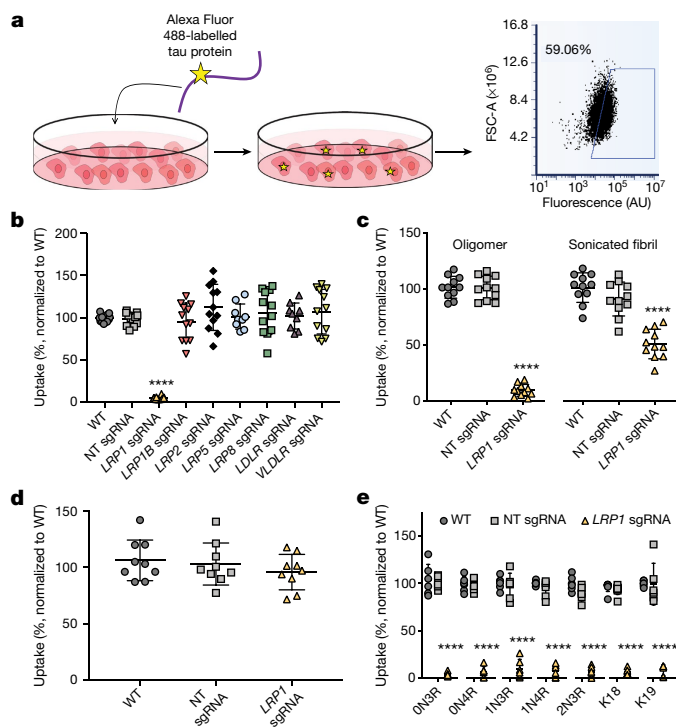


Fig. 1 | Tau uptake is mediated by LRP1. **a**, Left, diagram of the tau uptake assay. Fluorescently labelled tau is added to the cellular medium where it can be endocytosed by cells. Right, the uptake of tau can be measured via fluorescence using flow cytometry of single cells; see Methods for more details. FSC-A, forward scatter area. **b**, Measurement of tau uptake by flow cytometry (50 nM, 1 h) in H4 neuroglioma cells in which various LDLR family proteins have been knocked down by CRISPRi (H4i cells). NT sgRNA, non-targeting single-guide RNA ($n=12$; for *LRP5* and *LDLR*, $n=9$); WT, wild type. **c**, Endocytosis of tau oligomers (50 nM) and sonicated tau fibrils (100 nM) in H4i cells (1 h, $n=11$). **d**, Transferrin uptake (500 nM, 1 h, $n=9$) in H4i cells (ANOVA; $P=0.4464$). **e**, Endocytosis of tau isoforms (50 nM, 1 h, $n=6$; K18, $n=9$) in H4i cells. All experiments in **b–e** were performed as biological replicates over three independent experiments and normalized to wild-type uptake (100%). All data are expressed as mean \pm s.d. with individual data points shown. One-way ANOVA with Tukey's method, two-sided was performed to determine significance. Displayed are the comparisons against the wild type; **** $P<0.0001$. Comparison with NT sgRNA resulted in the same level of statistical significance.

ligands. Each complement-type repeat is composed of approximately 40 amino acids: six cysteines and a cluster of acidic residues (normally aspartic acid) that coordinates Ca^{2+} and interacts with lysine residues on ligands through salt bridges¹³. Tau has a high lysine content—out of 441 amino acids, 44 (about 10%) are lysines, 20 of which are located within the microtubule-binding region (the lysine content of the K18 fragment is around 15%). Furthermore, cryo-electron microscopy structures of tau fibrillar aggregates from the brains of patients with Alzheimer's disease or chronic traumatic encephalopathy^{14,15} show 10 or 11 resolved lysines, with all but one exposed to the exterior and therefore available for interactions with other proteins. To assess whether salt bridges between tau lysines and LRP1 were necessary for tau uptake, we capped all lysine residues on the K18 fragment using a sulfo-NHS acetate (NHS, *N*-hydroxysuccinimide) and measured endocytosis. The capping of lysine residues on K18 prevented the uptake of tau in wild-type H4 cells (Fig. 2b), which indicates that—similar to other LRP1 ligands—lysine residues are critical for this interaction.

LRP1 is a large (600 kDa) member of the LDLR family, and it contains 31 complement-type repeats divided into four different ligand-binding domains¹⁶. To elucidate which of these ligand-binding domains

influences tau uptake, we designed ectodomain constructs—known as mini-LRPs (mLRPs)—to assess the ability of individual subdomains (Fig. 2c) to rescue tau internalization in our *LRP1*-knockdown cells. By expressing these mLRPs in the absence of full-length LRP1 (Extended Data Fig. 2c), we found that full-length tau uptake was completely rescued with subdomain 4 (mLRP4) and partially rescued with mLRP2 (Fig. 2d). Furthermore, mLRP4 was able to co-immunoprecipitate tau, which confirms an interaction between the two (Extended Data Fig. 2d). Only mLRP4 improved K18 uptake (Fig. 2e), indicating that two motifs in tau could possess the ability to bind LRP1: one within the microtubule-binding region (amino acids 244–372) that interacts with mLRP4, and one in the N-terminal half (amino acids 1–243) or the C-terminal end (amino acids 373–441) that interacts with mLRP2. To test this further we examined the uptake of the N terminus of tau (amino acids 1–243), and found that both mLRP4 and (to a lesser extent) mLRP2 could rescue N-terminal uptake (Fig. 2f). This suggests a model in which a primary interaction site on mLRP4 mediates tau uptake, but that the N terminus of tau can also mediate interactions with a secondary site on mLRP2. We also noted that, although *LRP1* knockdown was sufficient to reduce uptake of the N terminus of tau, we did not observe the marked inhibition that was seen with constructs containing the microtubule-binding repeat region. This might be attributed to the higher concentrations of the N terminus that are required under our experimental conditions (Extended Data Fig. 2e), and could suggest that there is a secondary route of tau endocytosis, mediated by a slower, LRP1-independent pathway. To determine whether other known ligands of mLRP2 and mLRP4 are able to compete for uptake, we overexpressed various ApoE isoforms in HEK293T cells and collected the conditioned medium containing ApoE (Extended Data Fig. 2f). The results showed that incubation of H4 cells in ApoE conditioned medium significantly reduced the uptake of full-length tau, yet failed to reduce transferrin uptake (Extended Data Fig. 2g).

Native LRP1 is highly expressed in neurons at the post-synaptic density^{17,18}, and previous work has highlighted that the spread of tau in vivo is probably mediated trans-synaptically. Therefore, we asked whether the uptake of tau in neurons was also regulated by LRP1. We reduced the expression of *LRP1* in human induced pluripotent stem cell-derived neurons (iPSNs) using CRISPRi (Extended Data Fig. 3a). Micrographs of adherent iPSNs showed that *LRP1* knockdown efficiently reduced the amount of internalized tau (Tau-488, green; Fig. 3a). Quantification of tau endocytosis by flow cytometry confirmed the reduction of tau uptake upon *LRP1* knockdown, or upon the addition of RAP—but not mtRAP—into the culture medium (Fig. 3b, c). Similar to the results in H4 cells, *LRP1* knockdown or the addition of RAP had no effect on transferrin uptake in iPSNs (Fig. 3c).

On the basis of these in vitro results, we sought to determine whether LRP1 was also critical for the spread of tau in the brain. A recently described model of tau spread uses an adeno-associated virus (AAV) and enables reliable discrimination between neurons that have been transduced to express human tau (hTau) and neurons that receive hTau through spread¹⁹. The AAV encodes one mRNA—GFP-P2A-hTau under the control of a cytomegalovirus promoter—but produces two proteins, GFP and hTau (Fig. 4a). The P2A peptide self-cleaves during translation²⁰—as such, transduced neurons can be identified by the presence of GFP and hTau, whereas cells that have taken up tau via spread mechanisms can be identified by the absence of GFP and the presence of hTau (Fig. 4a). To regulate the expression of *LRP1* in parallel, an AAV (PHP.eB serotype) carrying a short hairpin RNA (shRNA) targeting *LRP1* under the human synapsin promoter was used to knock down *LRP1* in neurons (Extended Data Fig. 3b, d). We administered AAVs encoding either the shRNA targeting *LRP1* or a control 'scramble' shRNA through retro-orbital injection into six-week-old wild-type mice, and two weeks later we administered stereotactic injections of the AAV GFP-P2A-hTau virus into the hippocampus. After three weeks of incubation, the mice were euthanized

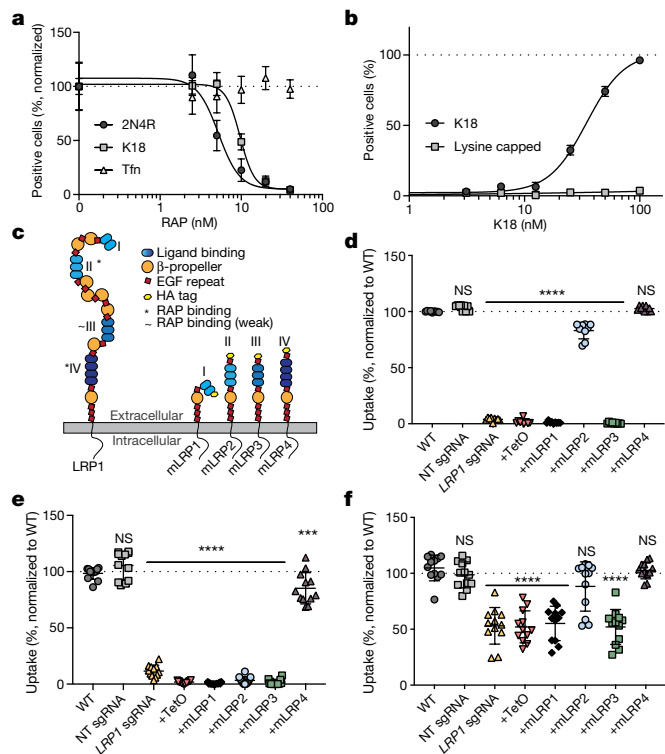


Fig. 2 | Tau interacts with LRP1 in a similar manner to known ligands.

a, Uptake of K18, 2N4R tau and transferrin (Tfn) in the presence of increasing RAP concentrations in the cell medium. **b**, Uptake of K18 and lysine-capped K18 in wild-type H4 cells. **c**, Schematic of LRP1 ectodomains. EGF, epidermal growth factor. **d**, Uptake of 2N4R tau with mLRP ectodomain expression ($n = 9$; WT versus NT, $P = 0.2232$; WT versus mLRP4, $P = 0.5450$). TetO, empty vector control. **e**, Uptake of K18 with mLRP ectodomain expression ($n = 12$; WT versus NT, $P = 0.2648$; WT versus mLRP4, $P = 0.0006$). **f**, Uptake of the N terminus of tau with mLRP ectodomain expression ($n = 12$; WT versus NT, $P = 0.9713$; WT versus mLRP2, $P = 0.1289$; WT versus mLRP4, $P > 0.9999$). Experiments in **a**, **b** were performed as biological duplicates over three independent experiments ($n = 6$) and representative examples are shown. Experiments in **d–f** were performed as biological triplicates over at least three independent experiments and normalized to wild-type uptake (100%, indicated by lines). All data are expressed as mean \pm s.d. with individual data points shown. One-way ANOVA with Tukey's method, two-sided was performed to determine significance. Displayed is the multiple comparison against the wild type; NS, not significant; *** $P \leq 0.001$, **** $P < 0.0001$. Comparison with NT sgRNA resulted in the same level of statistical significance.

and spread was determined by immunofluorescence experiments (Fig. 4b, c). AAVs encoding scramble shRNA and shRNA against *LRP1* contained the fluorescent protein reporter mRuby, which enabled us to visualize their expression throughout the brain (Fig. 4b). Mice expressing shRNA against *LRP1* showed reduced expression for *LRP1*, as determined by quantitative PCR and immunohistochemistry analysis (Extended Data Fig. 3b, f). To quantify tau spread, the number of hTau⁺/GFP⁺ cells was counted after immunostaining for human tau (Fig. 4c, d). We observed a substantial amount of tau spread in mice injected with PBS and scramble shRNA (mean \pm s.d. 199 ± 73 and 147 ± 43 hTau⁺/GFP⁺ cells per mm², respectively), whereas spread was greatly diminished in *LRP1*-knockdown mice (19 ± 19 hTau⁺/GFP⁺ cells per mm²) (Fig. 4d). This was not due to differences in the number of transduced cells, as we observed equivalent amounts of GFP⁺ cells across all mice (Fig. 4e). When analysing tau spread by brain region, we found that whereas mice injected with shRNA against *LRP1* had similar numbers of spread cells in the ipsilateral hippocampus (Fig. 4f), spread was significantly diminished in the cortex (Fig. 4g, i).

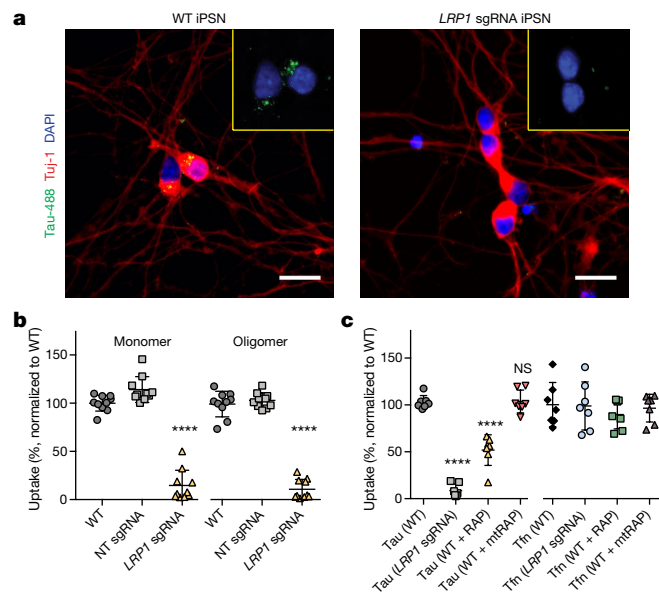


Fig. 3 | LRP1 mediates tau uptake in neurons. **a**, Representative images of wild-type iPSNs or iPSNs treated with *LRP1* sgRNA after tau uptake. Green, Tau-488; red, neuronal marker Tuj-1; blue, DAPI; scale bars, 20 μ m. **b**, Uptake of 2N4R monomers and oligomers in the stated iPSNs ($n = 10$ per condition). **c**, Uptake of 2N4R tau (WT versus mtRAP, $P > 0.9999$) or Tfn (ANOVA; $P = 0.7815$) in the presence of RAP or mtRAP ($n = 7$). All experiments in **a–c** were performed over three independent experiments and normalized to wild-type uptake (100%). Data are expressed as mean \pm s.d. with individual data points shown. One-way ANOVA with Tukey's method, two-sided was performed to determine significance. Displayed is the multiple comparison against the wild type; NS, not significant; **** $P < 0.0001$. Comparison with NT sgRNA resulted in the same level of statistical significance.

We observed no effect of sex on the spread phenotype (Extended Data Fig. 3c). *LRP1* is highly expressed in neurons, but it has also been shown to be present in other cell types including astrocytes and microglia²¹. Although not a focus of this work, we did observe instances of hTau⁺ astrocytes (Extended Data Fig. 3e); this will be a topic of future studies. Consistent with previous reports¹⁹, we found examples of MC-1 (an antibody recognizing an altered conformation of tau) reactivity in mice injected with PBS and scramble shRNA (Fig. 4h). Tau spread was also observed in the contralateral hippocampus of such mice, but was absent in mice injected with shRNA against *LRP1* (Fig. 4j).

Our study identifies *LRP1* as a master regulator of tau protein endocytosis in neurons, with an important role in the spread of tau in the brain. Targeting neuronal *LRP1* led to a significant reduction of tau spread in vivo, and could point to a new therapeutic approach for tau-related neurodegenerative diseases. The importance of *LRP1* in Alzheimer's disease has previously been attributed to its regulatory role in both the degradation and production of amyloid- β , and the internalization of ApoE²². ApoE4 has been shown to exacerbate amyloid- β pathology in a manner that depends on *LRP1* expression²³, and has also been found to worsen tau pathology²⁴. ApoE4 is known to have the lowest levels of circulating protein in the brain relative to the other ApoE isoforms²⁵, which suggests that it would be the least effective at inhibiting tau–*LRP1* interactions and, therefore, at suppressing tau spread. Together, our results point to *LRP1* as a common factor that can help to explain the co-occurrence of amyloid and tau lesions. Recently, tau uptake studies have focused on mechanisms dependent on HSPGs^{5,6}. However, HSPGs are known to act both independently and together with co-receptors to mediate endocytosis²⁶. This work therefore improves our understanding of tau spread, highlights *LRP1* as a critical determinant

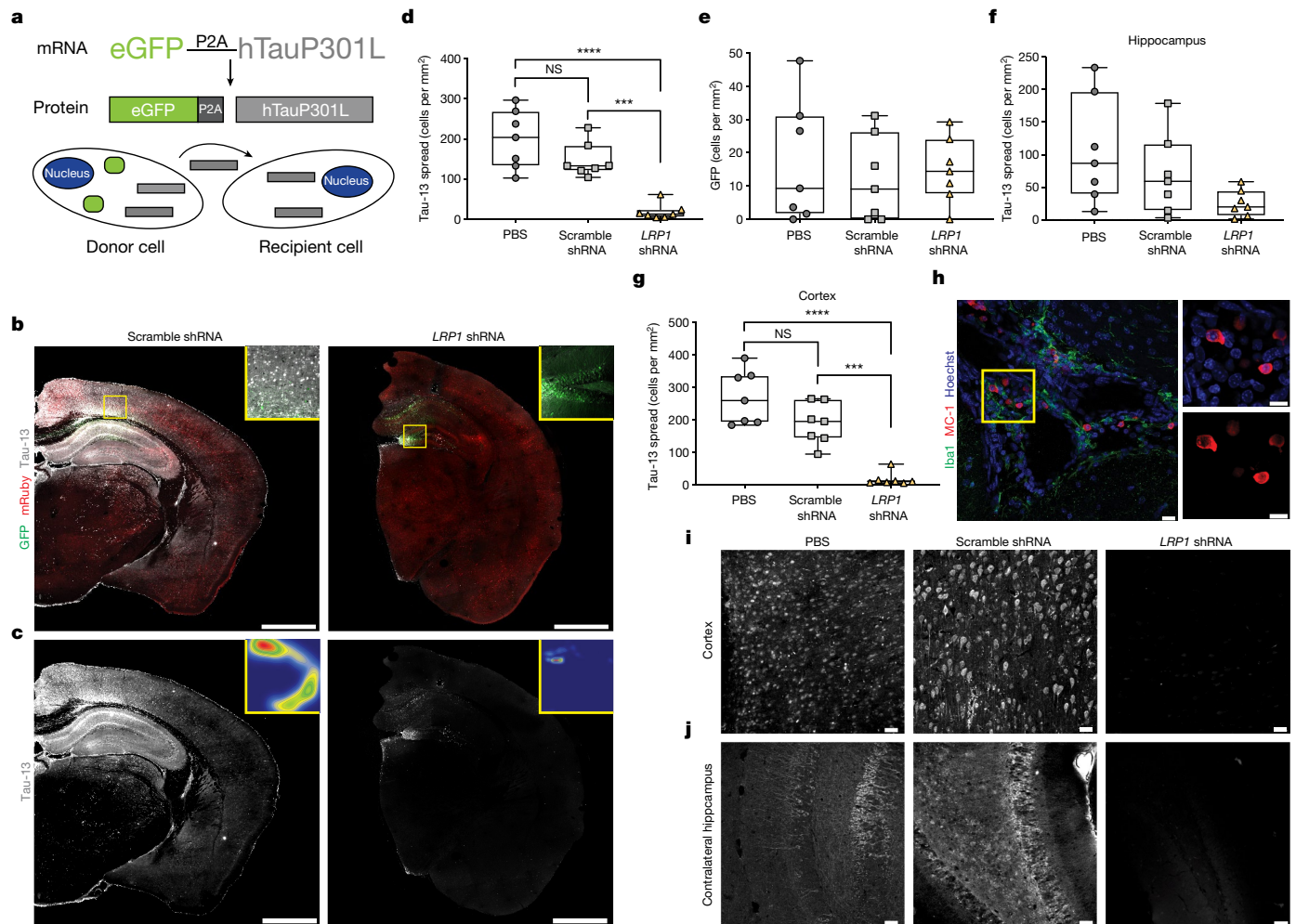


Fig. 4 | LRP1 knockdown reduces tau spread in vivo. **a**, Diagram of the AAV method used to study tau spread in vivo. **b**, Representative mosaic of a mouse injected with scramble shRNA (left) and a mouse injected with LRP1 shRNA (right), insets show a magnified view near the injection site. Green, GFP; red, shRNA; white, hTau; scale bars, 1 mm. **c**, hTau spread in mice injected with either scramble shRNA (left) or LRP1 shRNA (right), insets represent false-colour densitometric maps of hTau staining. Scale bars, 1 mm. **d**, Quantification of hTau⁺/GFP⁺ cells per mm² in mice injected with PBS, scramble shRNA or LRP1 shRNA (ANOVA; $P = 0.1582$). **e**, Quantification of GFP⁺ cells per mm² in mice injected with PBS, scramble shRNA or LRP1 shRNA (ANOVA; $P = 0.8007$). **f**, Quantification of ipsilateral hippocampal hTau⁺/GFP⁺ cells per mm² in mice injected with PBS, scramble shRNA or LRP1 shRNA (ANOVA; $P = 0.0692$). **g**, Quantification of ipsilateral cortical hTau⁺/GFP⁺ cells per mm² in

mice injected with PBS, scramble shRNA or LRP1 shRNA (PBS versus scramble shRNA, $P = 0.0548$). **h**, Image of MC-1⁺ tau in a PBS-injected mouse (green, Iba1; red, MC-1; blue, Hoechst; scale bars, 20 μ m). **i**, Representative images of ipsilateral cortex from mice injected with PBS, scramble shRNA or LRP1 shRNA (white, hTau; scale bars, 20 μ m). **j**, Representative images of contralateral hippocampus from mice injected with PBS, scramble shRNA or LRP1 shRNA (white, hTau; scale bars, 20 μ m). Experiments in **b–j**, $n = 7$ mice for each group (PBS, scramble shRNA, LRP1 shRNA). Data are shown as box plots with the median displayed as a line and the whiskers representing the minimum and maximum values. One-way ANOVA with Tukey's method, two-sided was performed to determine significance; NS, not significant; *** $P \leq 0.001$, **** $P < 0.0001$.

for tau propagation and suggests that interventions along a single pathway or at a single nidus—in which tau, ApoE and HSPGs operate dynamically in conjunction with LRP1—may remediate both plaque and tangle pathologies.

Online content

Any methods, additional references, Nature Research reporting summaries, source data, extended data, supplementary information, acknowledgements, peer review information; details of author contributions and competing interests; and statements of data and code availability are available at <https://doi.org/10.1038/s41586-020-2156-5>.

- Goedert, M., Eisenberg, D. S. & Crowther, R. A. Propagation of tau aggregates and neurodegeneration. *Annu. Rev. Neurosci.* **40**, 189–210 (2017).

- Braak, H. & Braak, E. Neuropathological staging of Alzheimer-related changes. *Acta Neuropathol.* **82**, 239–259 (1991).
- de Calignon, A. et al. Propagation of tau pathology in a model of early Alzheimer's disease. *Neuron* **73**, 685–697 (2012).
- Guo, J. L. et al. Unique pathological tau conformers from Alzheimer's brains transmit tau pathology in nontransgenic mice. *J. Exp. Med.* **213**, 2635–2654 (2016).
- Rauch, J. N. et al. Tau internalization is regulated by 6-O sulfation on heparan sulfate proteoglycans (HSPGs). *Sci. Rep.* **8**, 6382 (2018).
- Holmes, B. B. et al. Heparan sulfate proteoglycans mediate internalization and propagation of specific proteopathic seeds. *Proc. Natl Acad. Sci. USA* **110**, E3138–E3147 (2013).
- Kanekiyo, T. et al. Heparan sulphate proteoglycan and the low-density lipoprotein receptor-related protein 1 constitute major pathways for neuronal amyloid- β uptake. *J. Neurosci.* **31**, 1644–1651 (2011).
- Evans, L. D. et al. Extracellular monomeric and aggregated tau efficiently enter human neurons through overlapping but distinct pathways. *Cell Rep.* **22**, 3612–3624 (2018).
- De Nardis, C. et al. Recombinant expression of the full-length ectodomain of LDL receptor-related protein 1 (LRP1) unravels pH-dependent conformational changes and the stoichiometry of binding with receptor-associated protein (RAP). *J. Biol. Chem.* **292**, 912–924 (2017).

10. Dolmer, K., Campos, A. & Gettins, P. G. Quantitative dissection of the binding contributions of ligand lysines of the receptor-associated protein (RAP) to the low density lipoprotein receptor-related protein (LRP1). *J. Biol. Chem.* **288**, 24081–24090 (2013).
11. Nikolic, J. et al. Structural basis for the recognition of LDL-receptor family members by VSV glycoprotein. *Nat. Commun.* **9**, 1029 (2018).
12. Fisher, C., Beglova, N. & Blacklow, S. C. Structure of an LDLR-RAP complex reveals a general mode for ligand recognition by lipoprotein receptors. *Mol. Cell* **22**, 277–283 (2006).
13. Lillis, A. P., Van Duyn, L. B., Murphy-Ullrich, J. E. & Strickland, D. K. LDL receptor-related protein 1: unique tissue-specific functions revealed by selective gene knockout studies. *Physiol. Rev.* **88**, 887–918 (2008).
14. Fitzpatrick, A. W. P. et al. Cryo-EM structures of tau filaments from Alzheimer's disease. *Nature* **547**, 185–190 (2017).
15. Falcon, B. et al. Novel tau filament fold in chronic traumatic encephalopathy encloses hydrophobic molecules. *Nature* **568**, 420–423 (2019).
16. Xing, P. et al. Roles of low-density lipoprotein receptor-related protein 1 in tumors. *Chin. J. Cancer* **35**, 6 (2016).
17. Andersen, O. M. & Willnow, T. E. Lipoprotein receptors in Alzheimer's disease. *Trends Neurosci.* **29**, 687–694 (2006).
18. Nakajima, C. et al. Low density lipoprotein receptor-related protein 1 (LRP1) modulates N-methyl-D-aspartate (NMDA) receptor-dependent intracellular signaling and NMDA-induced regulation of postsynaptic protein complexes. *J. Biol. Chem.* **288**, 21909–21923 (2013).
19. Wegmann, S. et al. Experimental evidence for the age dependence of tau protein spread in the brain. *Sci. Adv.* **5**, eaaw6404 (2019).
20. Szymczak, A. L. et al. Correction of multi-gene deficiency in vivo using a single 'self-cleaving' 2A peptide-based retroviral vector. *Nat. Biotechnol.* **22**, 589–594 (2004).
21. Auderset, L., Cullen, C. L. & Young, K. M. Low density lipoprotein-receptor related protein 1 is differentially expressed by neuronal and glial populations in the developing and mature mouse central nervous system. *PLoS ONE* **11**, e0155878 (2016).
22. Shinohara, M., Tachibana, M., Kanekiyo, T. & Bu, G. Role of LRP1 in the pathogenesis of Alzheimer's disease: evidence from clinical and preclinical studies. *J. Lipid Res.* **58**, 1267–1281 (2017).
23. Tachibana, M. et al. APOE4-mediated amyloid- β pathology depends on its neuronal receptor LRP1. *J. Clin. Invest.* **129**, 1272–1277 (2019).
24. Shi, Y. et al. ApoE4 markedly exacerbates tau-mediated neurodegeneration in a mouse model of tauopathy. *Nature* **549**, 523–527 (2017).
25. Mahley, R. W. Central nervous system lipoproteins: ApoE and regulation of cholesterol metabolism. *Arterioscler. Thromb. Vasc. Biol.* **36**, 1305–1315 (2016).
26. Christianson, H. C. & Belting, M. Heparan sulfate proteoglycan as a cell-surface endocytosis receptor. *Matrix Biol.* **35**, 51–55 (2014).

Publisher's note Springer Nature remains neutral with regard to jurisdictional claims in published maps and institutional affiliations.

© The Author(s), under exclusive licence to Springer Nature Limited 2020

Methods

Cloning

Single-guide RNA (used for dCas9-KRAB gene repression) constructs for individual genes were cloned into the pLG15 vector, according to previously published methods²⁷. mLRP constructs were cloned into a pIRES-EGFP-puro (Addgene, 45567) from human cDNA. All mLRP constructs contained the N-terminal signalling peptide, residues 1–5, haemagglutinin (HA) tag, and the C-terminal transmembrane domain/tail (residues 3765–4525)²⁸. Individual mLRP constructs were cloned to contain their respective subdomains in between the HA tag and the C-terminal domain (mLRP1 residues 6–94; mLRP2 residues 787–1164; mLRP3 residues 2462–2923; mLRP4 residues 3264–3764). RAP was cloned into the pMCSG7 vector from human cDNA. Mutagenesis was performed on various constructs under standard protocols. Correct DNA sequences were confirmed (Genewiz).

Protein purification and labelling

Tau proteins were purified as described previously⁵. RAP, mtRAP, and the N terminus of tau were cloned into the pMCSG7 and purified on nickel-nitrilotriacetic acid (Ni-NTA) agarose (Qiagen). The His-tag was removed by tobacco etch virus (TEV) protease cleavage and subsequent clean-up on Ni-NTA agarose. Transferrin was purchased from Millipore and labelled in-house. Protein was labelled with Alexa Fluor 488 or 647 5-SDP ester (Life Technologies) according to the supplier's instructions. After labelling, 100 mM glycine was added to quench the reaction and the proteins were subjected to Zeba desalting columns (Thermo Scientific) to remove any unreacted label. Average label incorporation was between 1 and 1.5 moles per mole of protein, as determined by measuring fluorescence and protein concentration ($A_{\text{max}} \times \text{molecular mass of protein} / [\text{protein}] \times \epsilon_{\text{dye}}$, where A_{max} is the absorbance measured at the maximum absorption wavelength and ϵ_{dye} is the molar extinction coefficient of the dye). Lysine capped proteins were prepared with Sulfo-NHS-Acetate (Thermo) according to the manufacturer's instructions. Phosphorylation of tau was achieved by incubation with mouse brain extract in accordance with published work²⁹ and confirmed via western blotting. To prepare tau fibrils and oligomers, 10 μM protein, in PBS 1 mM DTT pH 7.4, was mixed with heparin (0.05 mg ml^{-1}) and incubated with shaking at 37 °C. The formation of oligomers was observed after 4 h of shaking, whereas fibril formation occurred after 5 days as previously described³⁰. To make sonicated fibril samples, fibrillized protein was sonicated using a Model 120 Sonicator (Fisher) at 30% amplitude for 30 \times 1 s pulses.

Cell culture

Cell lines (H4, HEK293T) were obtained from the American Type Culture Collection (ATCC) and were maintained in DMEM supplemented with 10% FBS, 100 $\mu\text{g ml}^{-1}$ penicillin/streptomycin. H4 cells constitutively expressing CRISPRi machinery (H4i)⁵ were cultured in DMEM supplemented with 10% FBS and 100 $\mu\text{g ml}^{-1}$ penicillin/streptomycin. Cultures were maintained in a humidified atmosphere of 5% CO_2 at 37 °C. H4i cells were infected with indicated sgRNA constructs and selected with puromycin (1 $\mu\text{g ml}^{-1}$). Knockdown was confirmed by quantitative PCR and western blot analysis using anti-LRP1 (Sigma L2295; 1:1,000) and anti-actin (Sigma A5441; 1:10,000) as a loading control (Extended Data Fig. 1b, d). *LRP1* sgRNA H4i cells were infected with mLRP constructs and sorted for GFP expression using a SH800 cell sorter (Sony Biotechnology). Expression of mLRP constructs was confirmed via western blot analysis using anti-HA primary antibody (Sigma H3663; 1:1,000) and anti-GAPDH (Abcam 181602; 1:10,000) as a loading control and quantification of surface expression was analysed via immunocytochemistry (Extended Data Fig. 2c). HEK293T cells were transfected with various ApoE pCMV4 constructs (Addgene, 87085-7) using Lipofectamine 2000 (Thermo Fisher) and conditioned medium was collected two days later. The presence of ApoE in the medium was

confirmed by western blot (anti-ApoE; Abcam 52607; 1:1,000; Extended Data Fig. 2f). Cells were not authenticated. Cells routinely tested negative for mycoplasma contamination.

iPS culturing and differentiation

CRISPRi iPS cells with a constitutive dCas9-BFP-KRAB and doxycycline-inducible neurogenin2 (Ngn2)³¹ were maintained in 6-well Matrigel (Corning) coated plates with E8 medium (STEMCELL Technologies) and split with ReLeSR (STEMCELL Technologies) at a 1:20 ratio every 4–5 days. To induce differentiation, cells were plated in 6-well Matrigel-coated plates with N2 predifferentiation medium (Knockout DMEM/F12, NEAA, N2, 10 ng ml^{-1} NT-3, 10 ng ml^{-1} BDNF, 1 $\mu\text{g ml}^{-1}$ mouse laminin) in the presence of doxycycline (2 $\mu\text{g ml}^{-1}$). Three days later, cells were lifted again and replated on poly-L-lysine-coated 24-well plates in Brain-Phys Neuronal medium (STEMCELL Technologies). iPS neurons were assayed between days 14–18 of maturity as described in the following section.

Tau uptake assay

H4 cells were plated at 50,000 cells per well and iPSN were plated at 100,000 cells per well in a 24-well plate. The next day the medium was replaced, and cells were treated with Alexa Fluor 488- or Alexa Fluor 647-labelled tau protein (50 nM) or Alexa Fluor 488-labelled transferrin (500 nM) for 1 h at 37 °C (unless otherwise indicated in the figure legends). Cells were then washed twice with PBS and trypsinized to lift cells from the plate. Lifted cells were analysed using an Accuri-C6 Flow Cytometer (BD Biosciences) and propidium iodide was used to exclude dead cells from the analysis (Extended Data Fig. 1a). Experiments were run in biological duplicates or triplicates and data was normalized to wild-type uptake to combine datasets from multiple experiments. Internalization controls are provided in Extended Data Fig. 1b. For RAP competition, recombinant RAP protein was added into the medium at indicated concentrations at the same time as labelled tau. For ApoE competition, ApoE-conditioned medium was used as the replacement medium before tau addition.

AAV production and purification

For shRNA, PHP.eB AAVs were generated and collected as previously described³². This engineered capsid enables efficient transduction of the central nervous system via the vasculature³³. Sequences for LRP1 shRNA (CCGGGCTGAACACATTCTTTGGTAACTCGAGTTACCAAAGAA TGTGTTTCAGCTTTTGTG), and scramble shRNA (CCGGCAACAAGATGA AGAGCACCAACTCGAGTTGGTGCTCTTCATCTTGTGTTTTGTG) were obtained from Sigma and were tested before AAV cloning in mouse primary culture. Purified viruses were concentrated, washed in PBS, sterile-filtered and titred using quantitative PCR. EGFP-2A-hTauP301L constructs were packaged into AAV2/8 (Massachusetts Eye and Ear Institute vector core).

Mice

All procedures were performed with approval from the Institutional Animal Care and Use Committee and in compliance with the National Institutes of Health Guide for the Care and Use of Laboratory Animals, the Animal Welfare Act, and guidelines from the University of California, Santa Barbara. Mice were maintained in ventilated cages, on a standard rodent diet of chow and water ad libitum and housed under a 12-hour light/dark cycle.

Experiments were performed starting at 6 weeks of age on a sex-mixed (4 males and 3 females per condition) cohort of in-house bred mice (FVB/B6). Mice were injected retro-orbitally with either PBS or an AAV PHP.eB of mRuby-shRNA with either a scramble or LRP1 sequence. After two weeks, mice were intracranially injected with AAVs encoding EGFP-2A-hTauP301L into the hippocampus (1.5 μl unilaterally). Injections were performed under standard aseptic surgery conditions. Mice were anaesthetized with isoflurane (2%) and injections were made at

the coordinates (from bregma A/P −2 mm, M/L −1.5 mm, D/V −1.5 mm). A Hamilton needle was used to inject the AAV solution at 0.5 $\mu\text{l min}^{-1}$. Afterwards, the skin over the injection site was sutured and mice were allowed to recover on a warming pad. Mice received meloxicam for two days after surgery. No calculations were performed to predetermine sample size, sample sizes were based on previously published work and were chosen to support meaningful conclusions, and no specific method of randomization was used.

Immunohistochemistry

Mice were perfused using 4% paraformaldehyde in 0.1 M sodium cacodylate pH 7.4 for 15 min at room temperature. Brains were then immersion-fixed for 48 h at 4 °C. Immunocytochemistry was performed as described elsewhere³⁴; in brief, samples were rinsed 3 × 5 min, 1 × 1 h in cold phosphate buffered saline (PBS; pH: 7.4) and then sectioned at 100 μm using a vibratome (Leica). Sections were immersed in normal donkey serum (Jackson ImmunoResearch Laboratories) 1:20 in PBS containing 0.5% BSA, 0.1% Triton-X 100, and 0.1% sodium azide (PBTA) at 4 °C on a rotator with overnight agitation. Next, sections were immersed in primary antibodies, anti-Tau13 (Biolegend 835201; 1:200), anti-Iba1 (Wako laboratory chemicals 019-19741; 1:200), MC-1 (Peter Davies; 1:200), and anti-Sox2 (Abcam 97959; 1:200) diluted in PBTA. Subsequently, sections were rinsed in PBTA 5 × 5 min, 1 × 1 h in PBTA and then placed in corresponding secondary antibodies (Jackson ImmunoResearch Laboratories; 1:200). Last, sections were rinsed and mounted using Vectashield (Vector Laboratories) on a glass slide and sealed under a No. 0 coverslip (Thomas Scientific) using nail polish.

Large-scale mosaic acquisition and image registration

Samples were imaged using an Olympus FV1000 confocal microscope equipped with a precision motorized stage (Applied Scientific Instrumentation). Mosaics were captured using an UPlanSapo 20× oil immersion lens with numerical aperture 0.85 at 1- μm intervals in the z-dimension and a pixel display of 800 × 800 along the x–y axes. Image stacks were collected sequentially using the Olympus Fluoview software v.4.2 with 5% overlap between individual tiles. Image registration of individual z-stacks was performed in a semi-automated fashion using the bio-image software Imago 1.5 (Mayachitra). False-colour densitometric maps were generated using x, y coordinates from annotated images using the visualization open source package ggplot2 version 3.2.1 as part of RStudio desktop v.1.2.5001 and subsequently rendered using R v.3.6.1. Animal mosaics were quantified under blinding conditions, file names were withheld until after image analysis was completed.

Statistical analysis

All statistical analysis was performed using Prism 8 software. To determine statistical significance, Shapiro–Wilk tests were first used to evaluate the assumption of normality of the data. Given $P > 0.05$, then normality assumptions were not rejected and ANOVA tests were used. In certain cases, outliers were removed to meet the normality assumption and then an ANOVA test was performed; however, all data are displayed

in full. Post-hoc analysis of ANOVA was performed using Tukey's method in order to compare experimental samples to both wild-type and non-targeting sgRNA (or scramble shRNA) controls. For quantitative PCR data, unpaired *t*-tests were used to determine significance.

Reporting summary

Further information on research design is available in the Nature Research Reporting Summary linked to this paper.

Data availability

Source data are available for graphs plotted in Figs. 1–4 and Extended Data Figs. 1–3. Scans of the full western blot gels can be found in Supplementary Fig. 1. All other data are available from the corresponding author upon reasonable request.

27. Horlbeck, M. A. et al. Compact and highly active next-generation libraries for CRISPR-mediated gene repression and activation. *eLife* **5**, e19760 (2016).
28. Obermoeller-McCormick, L. M. et al. Dissection of receptor folding and ligand-binding property with functional minireceptors of LDL receptor-related protein. *J. Cell Sci.* **114**, 899–908 (2001).
29. Despres, C. et al. Identification of the tau phosphorylation pattern that drives its aggregation. *Proc. Natl Acad. Sci. USA* **114**, 9080–9085 (2017).
30. Usenovic, M. et al. Internalized tau oligomers cause neurodegeneration by inducing accumulation of pathogenic tau in human neurons derived from induced pluripotent stem cells. *J. Neurosci.* **35**, 14234–14250 (2015).
31. Tian, R. et al. CRISPR interference-based platform for multimodal genetic screens in human iPSC-derived neurons. *Neuron* **104**, 239–255 (2019).
32. Challis, R. C. et al. Systemic AAV vectors for widespread and targeted gene delivery in rodents. *Nat. Protoc.* **14**, 379–414 (2019).
33. Chan, K. Y. et al. Engineered AAVs for efficient noninvasive gene delivery to the central and peripheral nervous systems. *Nat. Neurosci.* **20**, 1172–1179 (2017).
34. Luna, G. et al. The effects of transient retinal detachment on cavity size and glial and neural remodeling in a mouse model of X-linked retinoschisis. *Invest. Ophthalmol. Vis. Sci.* **50**, 3977–3984 (2009).

Acknowledgements This study was funded by the National Institutes of Health (NIH), K99 AG064116 (J.N.R.), DP2 GM119139 (M.K.), R01 AG062359 (M.K.), R56 AG057528 (M.K.), U54 NS100717 (M.K., K.S.K.), Tau Consortium (M.K., K.S.K.), German Center for Neurodegenerative Diseases (S.W.), Ben Barres Early Career Acceleration Award from the Chan Zuckerberg Initiative (M.K.), Tri-counties Blood Bank (J.N.R.), Dr Miriam and Sheldon G. Adelson Medical Research Foundation (K.S.K.), Larry L. Hillblom Foundation (K.S.K.) and Edward N. & Della L. Thome Memorial Foundation (K.S.K.). We thank the Laboratory for Stem Cell Biology and Engineering at UCSB for use of their flow cytometer, the Neuroscience Research Institute Microscopy Facility for use of their microscopes, J. Dong for help in the early stages of this project and P. Davies for providing the MC-1 antibody.

Author contributions J.N.R. and K.S.K. conceived the study. J.N.R. and K.S.K. designed the study. J.N.R. performed most of the experiments and analysed the data, assisted by G.L., E.G., M.A., C.C., Y.E.S., C.L. and I.H. C.C., V.G., S.W. and B.T.H. provided AAVs used in the study. M.K. provided CRISPRi cell lines. J.N.R. and K.S.K. wrote the manuscript, and all authors discussed the results and commented on the manuscript.

Competing interests K.S.K. is on the Board of Directors of the Rainwater Charitable Trust.

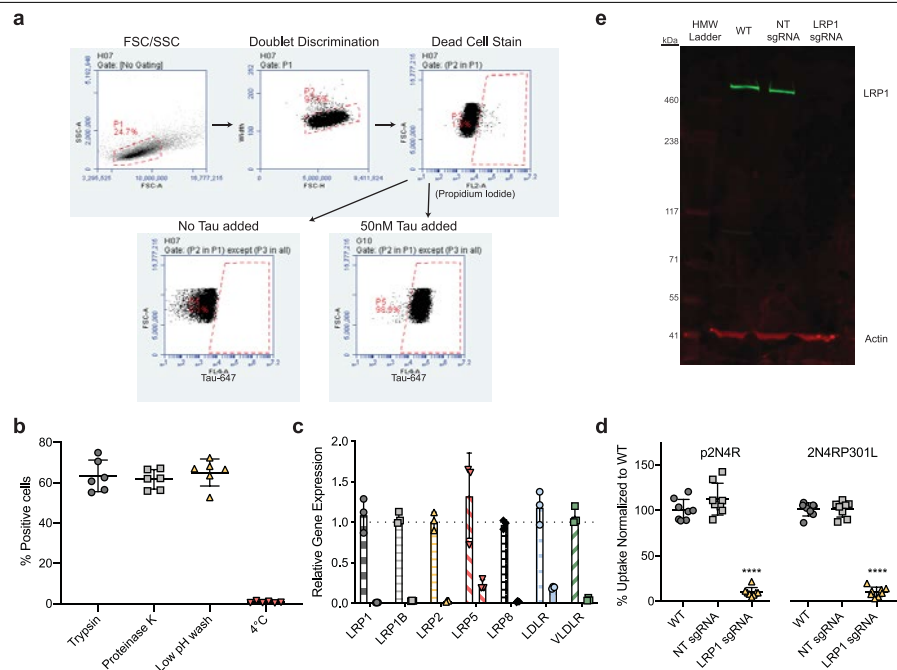
Additional information

Supplementary information is available for this paper at <https://doi.org/10.1038/s41586-020-2156-5>.

Correspondence and requests for materials should be addressed to K.S.K.

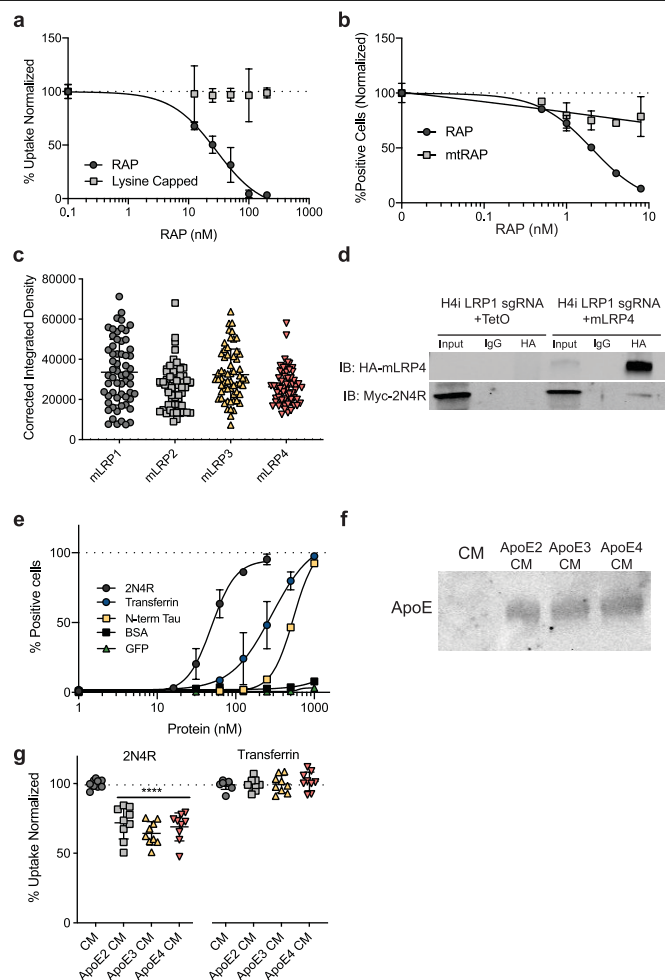
Peer review information Nature thanks Katrin Deinhardt, Joachim Herz and the other, anonymous, reviewer(s) for their contribution to the peer review of this work.

Reprints and permissions information is available at <http://www.nature.com/reprints>.

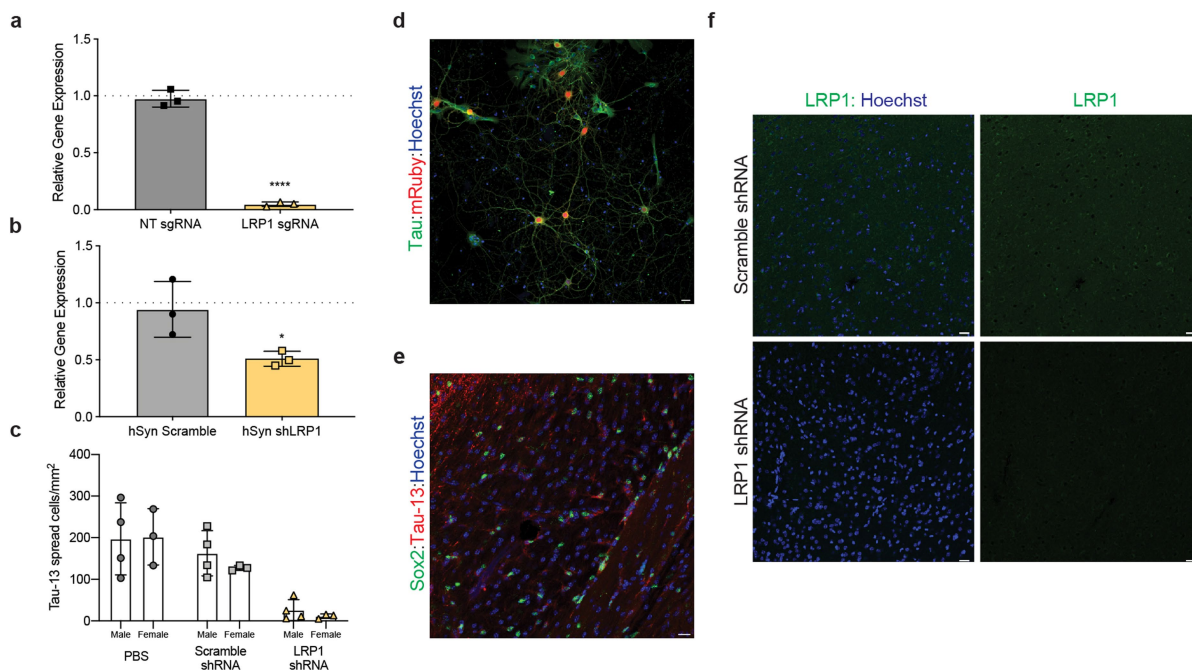


Extended Data Fig. 1 | Tau uptake is regulated by LRP1. **a**, Gating strategy for tau uptake assay. First, cells were gated on forward scatter/side scatter (FSC/SSC; mean FSC-A, around 8,000,000; mean SSC-A, around 800,000). Cells were then gated on forward scatter height (FSC-H) versus width to discriminate doublets. Dead cells were removed from the analysis using propidium iodide as a stain, and positive cells were determined by gating on a negative (no tau added) population. **b**, Internalization controls for tau uptake assay ($n = 6$). **c**, Quantitative PCR analysis of various genes with sgRNA in H4i

cells. The first column represents the NT sgRNA control for each target ($n = 3$). **d**, Uptake of phosphorylated (p2N4R) or mutated (2N4RP301L) full-length tau in H4i cells ($n = 8$). **e**, Western blot analysis of LRP1 in wild-type, NT sgRNA or LRP1 sgRNA H4i cells. All results in **b–e** were obtained in three independent experiments and normalized to wild-type uptake (100%). Data are expressed as mean \pm s.d. with individual data points shown. One-way ANOVA with Tukey's method, two-sided was performed to determine significance; **** $P < 0.0001$.



Extended Data Fig. 2 | LRP1 ligands influence tau uptake. a, Uptake of 2N4R tau with competition from RAP or lysine-capped RAP. **b**, Uptake of 2N4R tau with competition from RAP or mtRAP. **c**, Corrected integrated density of surface HA staining for different ectodomain cell lines ($n = 60$). **d**, Co-immunoprecipitation of HA-mLRP4 with myc-2N4R ($n = 3$). **e**, Uptake of various ligands at indicated concentrations (1 h). **f**, Western blot analysis of conditioned medium (CM) from HEK293T cells, mock-treated or overexpressing ApoE ($n = 3$). **g**, Uptake of full-length tau and transferrin in conditioned medium from **f** ($n = 9$). All experiments in **a**, **b**, **e** were performed in biological duplicate over three independent experiments ($n = 6$) with representative experiments shown. Data are expressed as mean \pm s.d. with individual data points shown. One-way ANOVA with Tukey's method, two-sided was performed to determine significance; **** $P < 0.0001$.



Extended Data Fig. 3 | *LRP1* expression influences tau spread.

a, Quantitative PCR analysis of *LRP1* expression in iPSNs ($n=3$; $P<0.0001$).

b, Quantitative PCR analysis of *LRP1* expression from mouse cortex transduced with human synapsin (hSyn) scramble shRNA or *LRP1* shRNA ($n=3$; $P=0.0412$).

c, Quantification of tau spread in mice broken down by sex (males $n=4$, females $n=3$; two-way ANOVA, sex = NS, $P=0.5335$). **d**, Immunofluorescence of mouse primary culture transduced with AAVmRuby-hSyn-shLRP1 (green, Tau; red,

mRuby; blue, Hoechst; scale bar, 20 μm , $n=3$). **d**, Immunohistochemistry of hTau⁺ astrocytes in mice injected with PBS (green, Sox2; red, hTau; blue, Hoechst; scale bar, 20 μm , $n=3$). **e**, Immunohistochemistry of mice injected with scramble shRNA and *LRP1* shRNA (green, LRP1; blue; Hoechst, scale bars, 20 μm ; $n=3$). Unpaired *t*-test, two-tailed was performed to determine statistical significance for quantitative PCR in **a**, **b**; * $P\leq 0.05$, **** $P<0.0001$.

Reporting Summary

Nature Research wishes to improve the reproducibility of the work that we publish. This form provides structure for consistency and transparency in reporting. For further information on Nature Research policies, see [Authors & Referees](#) and the [Editorial Policy Checklist](#).

Statistics

For all statistical analyses, confirm that the following items are present in the figure legend, table legend, main text, or Methods section.

- | | |
|-------------------------------------|--|
| n/a | Confirmed |
| <input type="checkbox"/> | <input checked="" type="checkbox"/> The exact sample size (n) for each experimental group/condition, given as a discrete number and unit of measurement |
| <input type="checkbox"/> | <input checked="" type="checkbox"/> A statement on whether measurements were taken from distinct samples or whether the same sample was measured repeatedly |
| <input type="checkbox"/> | <input checked="" type="checkbox"/> The statistical test(s) used AND whether they are one- or two-sided
<i>Only common tests should be described solely by name; describe more complex techniques in the Methods section.</i> |
| <input checked="" type="checkbox"/> | <input type="checkbox"/> A description of all covariates tested |
| <input type="checkbox"/> | <input checked="" type="checkbox"/> A description of any assumptions or corrections, such as tests of normality and adjustment for multiple comparisons |
| <input type="checkbox"/> | <input checked="" type="checkbox"/> A full description of the statistical parameters including central tendency (e.g. means) or other basic estimates (e.g. regression coefficient) AND variation (e.g. standard deviation) or associated estimates of uncertainty (e.g. confidence intervals) |
| <input type="checkbox"/> | <input checked="" type="checkbox"/> For null hypothesis testing, the test statistic (e.g. F , t , r) with confidence intervals, effect sizes, degrees of freedom and P value noted
<i>Give P values as exact values whenever suitable.</i> |
| <input checked="" type="checkbox"/> | <input type="checkbox"/> For Bayesian analysis, information on the choice of priors and Markov chain Monte Carlo settings |
| <input checked="" type="checkbox"/> | <input type="checkbox"/> For hierarchical and complex designs, identification of the appropriate level for tests and full reporting of outcomes |
| <input checked="" type="checkbox"/> | <input type="checkbox"/> Estimates of effect sizes (e.g. Cohen's d , Pearson's r), indicating how they were calculated |

Our web collection on [statistics for biologists](#) contains articles on many of the points above.

Software and code

Policy information about [availability of computer code](#)

Data collection

BD Accuri C6 software was used to acquire flow cytometry data. Quantstudio Design and Analysis Software v1.4 was used to acquire qPCR data. Odyssey software was used to capture western blot images. Image stacks were collected sequentially using the Olympus Flouview software version 4.2 with 5% overlap between individual tiles.

Data analysis

Prism 8 was used to perform statistical analysis on all data presented. Image registration of individual z-stacks was performed in a semi-automated fashion using the bio-image software Imago 1.5 (Mayachitra Inc.).

For manuscripts utilizing custom algorithms or software that are central to the research but not yet described in published literature, software must be made available to editors/reviewers. We strongly encourage code deposition in a community repository (e.g. GitHub). See the Nature Research [guidelines for submitting code & software](#) for further information.

Data

Policy information about [availability of data](#)

All manuscripts must include a [data availability statement](#). This statement should provide the following information, where applicable:

- Accession codes, unique identifiers, or web links for publicly available datasets
- A list of figures that have associated raw data
- A description of any restrictions on data availability

An excel file containing source data for the following figures has been included with submission (Fig. 1B, 1C, 1D, 1E, 2A, 2B, 2D, 2E, 2F, 3B, 3C, 4D, 4E, 4F, 4G, Extended Data Fig. 1B, 1C, 1D, 2A, 2B, 2C, 2E, 2G, 3A, 3B, 3C). Fully scanned western blot gels can be found in the Supplementary Information. All other data available from the corresponding author upon reasonable request.

Field-specific reporting

Please select the one below that is the best fit for your research. If you are not sure, read the appropriate sections before making your selection.

☒ Life sciences ☐ Behavioural & social sciences ☐ Ecological, evolutionary & environmental sciences

For a reference copy of the document with all sections, see [nature.com/documents/nr-reporting-summary-flat.pdf](https://www.nature.com/documents/nr-reporting-summary-flat.pdf)

Life sciences study design

All studies must disclose on these points even when the disclosure is negative.

Sample size	No calculations were performed to predetermine sample size, sample sizes were based on previously published work and chosen to support meaningful conclusions. The sample size (n) of each experiment is provided in the figure captions.
Data exclusions	No animals or samples were excluded from the displayed datasets. To determine statistical significance, Shapiro-Wilk tests were first used to evaluate the assumption of normality of the data. Given a $p > 0.05$ then normality assumptions were not rejected and ANOVA tests were used. In certain cases, outliers were removed to meet the normality assumption and then an ANOVA test was performed, however data is displayed in full.
Replication	All in vitro experiments were performed in biological duplicates or triplicates over three independent experiments. In vivo analysis was performed on $n=7$ animals per experimental group. All replications were consistent across multiple experiments.
Randomization	No specific method of randomization was used. However, four male and three female animals were used in this study.
Blinding	Animal mosaics were quantified under blinding conditions, file names were withheld until after image analysis was completed.

Reporting for specific materials, systems and methods

We require information from authors about some types of materials, experimental systems and methods used in many studies. Here, indicate whether each material, system or method listed is relevant to your study. If you are not sure if a list item applies to your research, read the appropriate section before selecting a response.

Materials & experimental systems

n/a	Involved in the study
<input type="checkbox"/>	<input checked="" type="checkbox"/> Antibodies
<input type="checkbox"/>	<input checked="" type="checkbox"/> Eukaryotic cell lines
<input checked="" type="checkbox"/>	<input type="checkbox"/> Palaeontology
<input type="checkbox"/>	<input checked="" type="checkbox"/> Animals and other organisms
<input checked="" type="checkbox"/>	<input type="checkbox"/> Human research participants
<input checked="" type="checkbox"/>	<input type="checkbox"/> Clinical data

Methods

n/a	Involved in the study
<input checked="" type="checkbox"/>	<input type="checkbox"/> ChIP-seq
<input type="checkbox"/>	<input checked="" type="checkbox"/> Flow cytometry
<input checked="" type="checkbox"/>	<input type="checkbox"/> MRI-based neuroimaging

Antibodies

Antibodies used	anti-Tau13 (Biolegend, cat no. 835201; mouse 1:200), anti-Iba1 (Wako laboratory chemicals, cat no. 019-19741; rabbit 1:200), MC-1 (Peter Davies; mouse 1:200), anti-Tuj1 (Sigma cat no. T3952; rabbit 1:200), anti-HA (Sigma, cat no. H3663; mouse 1:1000), anti-GAPDH (Abcam, cat no. 181602; rabbit 1:10000), anti-LRP1 (Sigma, cat no. L2295; rabbit 1:1000), anti-actin (Sigma, cat no. A5441, mouse 1:10000), anti-ApoE (Abcam, cat no. 52607; rabbit 1:1000), anti-Sox2 (Abcam, cat no. 97959; rabbit 1:200), anti-myc (Cell signaling, cat no. 2272; rabbit 1:1000), anti-LRP1 (Abcam, cat no. 92544; rabbit 1:200).
Validation	All commercially purchased antibodies were validated for their respective application by their manufacturer. MC-1 antibody obtained from Peter Davies has been validated in the literature previously (Jicha et. al, J NeuroSci 1997).

Eukaryotic cell lines

Policy information about [cell lines](#)

Cell line source(s)	Cell lines (H4, HEK293T) were obtained from the ATCC. CRISPRi H4 and CRISPRi iPSc were provided by Martin Kampmann, UCSF (Tian, R. et al. CRISPR Interference-Based Platform for Multimodal Genetic Screens in Human iPSC-Derived Neurons. Neuron, doi:10.1016/j.neuron.2019.07.014 (2019))
Authentication	None of the cell lines have been authenticated.

Mycoplasma contamination	All cell lines used tested negative for mycoplasma contamination using a PCR Mycoplasma test kit (VWR 10181-030).
Commonly misidentified lines (See ICLAC register)	None used.

Animals and other organisms

Policy information about [studies involving animals](#); [ARRIVE guidelines](#) recommended for reporting animal research

Laboratory animals	Experiments were performed on six-week old mice, (FVB/B6, four males/three females were used for each experimental cohort).
Wild animals	The study did not involve wild animals.
Field-collected samples	The study did not involve samples collected from the field.
Ethics oversight	All procedures were done with approval from the Institutional Animal Care and Use Committee and in compliance with the National Institutes of Health Guide for the Care and Use of Laboratory Animals, the Animal Welfare Act, and guidelines from the University of California, Santa Barbara.

Note that full information on the approval of the study protocol must also be provided in the manuscript.

Flow Cytometry

Plots

Confirm that:

- ☒ The axis labels state the marker and fluorochrome used (e.g. CD4-FITC).
- ☒ The axis scales are clearly visible. Include numbers along axes only for bottom left plot of group (a 'group' is an analysis of identical markers).
- ☒ All plots are contour plots with outliers or pseudocolor plots.
- ☒ A numerical value for number of cells or percentage (with statistics) is provided.

Methodology

Sample preparation	Cells were obtained from culture conditions and were lifted and analyzed without fixation.
Instrument	BD Accuri C6 for routine analysis and Sony SH800 for sorting
Software	BD Accuri C6 software for collection and Prism 8 software for data analysis.
Cell population abundance	Cells that were infected with mLRP constructs were sorted using a Sony SH800 Cell Sorter on EGFP expression. Cells were sorted using a standard two-way sort. Cells were determined to be >99% positive after sorting.
Gating strategy	Cells were gated on FSC/SSC (Mean FSC-A: ~ 8,000,000/Mean SSC-A: ~800,000). Cells were gated on FSC-H vs. Width to discriminate doublets. Dead cells were removed from analysis using propidium iodide as a stain, and positive cells were determined by gating on a negative (no tau added) population. See Extended Data Fig. 1a.

- ☒ Tick this box to confirm that a figure exemplifying the gating strategy is provided in the Supplementary Information.